Available online at www.sciencedirect.com
SCIENCE DIRECT®
Journal of Nuclear Materials 334 (2004) 104–108
journal of nuclear materials
www.elsevier.com/locate/jnucmat

Creep properties of a reduced activation 9Cr3WVTaB martensitic steel after helium implantation

Toshinori Chuto *, Norikazu Yamamoto, Yoshiharu Murase, Johsei Nagakawa

National Institute for Materials Science, 1-2-1, Sengen, Tsukuba, Ibaraki 305-0047, Japan

Received 24 March 2003; accepted 5 April 2004

Abstract

Influence of helium on creep rupture properties of a reduced activation 9Cr3WVTaB martensitic steel for fusion applications has been examined. Homogeneous helium implantation using α-particle irradiation at an accelerator was adopted to simulate transmutational production of helium in fusion reactors. Helium was introduced into creep specimens at 600 °C with concentrations up to 300 appmHe. Creep rupture tests at the same temperature were carried out on specimens both with and without helium. Both creep lifetime and rupture elongation were not so much affected by helium. All the implanted specimens failed in a perfectly intragranular ductile manner without any indication of grain boundary separation induced by helium. These results indicate good resistance of the steel against high-temperature helium embrittlement.

1. Introduction

Reduced activation Fe–Cr–W–V–Ta martensitic steels are primary candidates for first wall and blanket components in future fusion power systems, mainly due to their maturity as industrial materials [1]. It has been reported that the family of these steels containing 7–9Cr, 2W, 0.2–0.3V and 0.03–0.1Ta (in weight percentage) exhibited good resistance to radiation damage [2–4], e.g. good tensile and impact properties after neutron irradiation in fission reactors and superior void swelling resistance. In fusion environment, especially in case of advanced systems, influence of transmutational helium, as well as that of displacement damage, on material properties is important because a large amount of helium which is generated through (n,α) reactions by energetic fusion neutrons often causes deterioration of high-temperature mechanical properties, so-called helium embrittlement. Such helium embrittlement at elevated temperature is known to appear more markedly in long-term experiments rather than short time examinations such as tensile tests [5,6]. Therefore long time inspections are crucial for investigation of helium-embrittlement resistance of materials. Excellent resistance to helium embrittlement was obtained for F82H, (7.5–8)Cr–2W–0.2V–0.03Ta–0.1C steel containing up to 1000 appmHe in creep rupture tests at 550 °C [7]. However, information about helium-embrittlement resistance of the steels is still very limited.

The highest operating temperature of the steels stated above is considered to be 550–600 °C that is most probably determined by coolant compatibility and/or creep. It is of interest from the economical point of view to improve high-temperature strength and increase the upper temperature performance limit of the steels for fusion power plants, and one possible way to do this is to increase tungsten content. The purpose of this study is to clarify the influence of helium on creep properties of a reduced activation 9Cr3WVTaB martensitic steel of which alloy composition was adjusted for improvement in high-temperature strength. The neutronic production of helium in fusion environment was simulated

* Corresponding author. Tel./fax: +81-29 859 2014.
E-mail address: chuto.toshinori@nims.go.jp (T. Chuto).

0022-3115/$ - see front matter © 2004 Elsevier B.V. All rights reserved.
doi:10.1016/j.jnucmat.2004.04.351

by homogeneous α-implantation at a cyclotron accelerator.

2. Experimental

The material studied was Fe–0.17C–9.2Cr–3.1W–0.16V–0.10Ta–0.007B steel (in weight percentage) that was fabricated in NIMS (National Institute for Materials Science) as a 17 kg ingot. Subsequent to hot forging, the ingot was hot-rolled with a grooved roll to square bars having a cross-section of 13×13 mm^2. The bars were cold-rolled to plates of 1.4 mm in thickness, and subjected to process annealing at 780 °C for 7.2 ks. The annealed plates were then cold-rolled to about 0.085 mm thick sheets. Creep test specimens with dimensions shown in Fig. 1 were punched out from the sheets. After polishing the surfaces on emery papers, thickness of the test samples was reduced to about 0.082 mm that was determined by the projective range of α-particles mentioned below. Final heat treatments were given by normalizing for 1.8 ks at 1100 °C and tempering for 3.6 ks at 800 °C, and they yielded fully martensitic structure with an austenitic grain size of 27 μm.

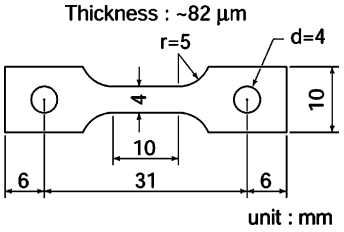

Fig. 1. Dimensions of creep specimen.

Helium implantation was carried out in a vacuum of about 3×10^{-4} Pa using a 20 MeV α-beam from the NIMS compact cyclotron. The projective range of the beam was calculated to be 82.5 μm on SRIM 96 code. A schematic view of the irradiation system in this study is illustrated in Fig. 2. The energy of α-particles was degraded with a rotating energy absorber consisting of Al foils with 16 different thicknesses in order to obtain homogeneous helium distribution along the injected direction in the specimen. In addition, the beam was scanned in the other two directions to achieve lateral homogeneity. The specimens were irradiated at 600 °C to helium contents of about 100 and 300 appm with dose rates of $1.4–1.7\times10^{-3}$ appmHe/s. Implantation temperature was measured with two thermocouples spot-welded on a dummy plate mounted in the middle of the irradiated area. Temperature change due to beam fluctuation was compensated by adopting an infra-red lamp heater with rapid response, and suppressed within 4 °C during each implantation. The difference of readings between left and right thermocouples was less than 15 °C. The amount of implanted helium was estimated on the basis of measured target current.

Creep rupture tests were carried out also at 600 °C in a vacuum of $<5\times10^{-5}$ Pa using electro-mechanically controlled machines. The details of the apparatus have been described in Ref. [8]. The shifts of temperature from the stated value were kept less than ±2 °C during creep tests. Applied stress was set between 183 and 222 MPa, and the deviation from the nominal stress was maintained less than ±1 MPa at each stress level. In addition to the implanted samples, series of creep tests at similar conditions were carried out on unimplanted reference specimens that underwent the same thermal histories as corresponding implanted ones. Control samples corresponding to 100 and 300 appmHe implantation were prepared by annealing at 600 °C for

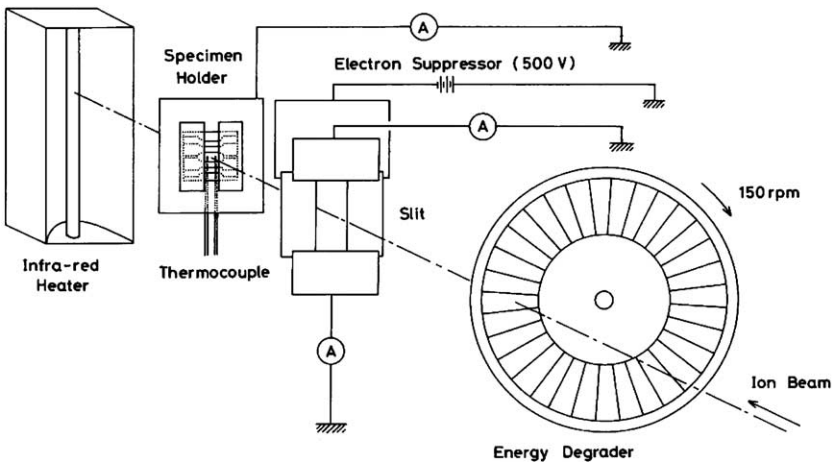

Fig. 2. Schematic illustration of helium implantation arrangement.

6.8×10^4 and 2.1×10^5 s, respectively, prior to creep rupture tests. After creep rupture tests, fracture surfaces of failed specimens were examined by scanning electron microscopy (SEM) in order to characterize the fracture mode.

3. Results and discussion

Fig. 3 compares typical creep curves between a helium-implanted specimen and an unirradiated control sample tested at almost the same applied stress for each implantation level. There was little difference in the creep rupture time between implanted and control specimens in case of 100 appmHe implantation, whereas the creep rupture time of the 300 appmHe implanted sample was somewhat shorter than that of corresponding control. The same is also shown in standard creep rupture plots. In Fig. 4, creep stress versus time to rupture relation on helium-implanted and control specimens is presented for both helium concentrations. The creep lifetime of the samples containing 100 appmHe was very close to that of corresponding controls. As for the 300 appmHe implantation, it is shown in the figure that the rupture time of the implanted samples was

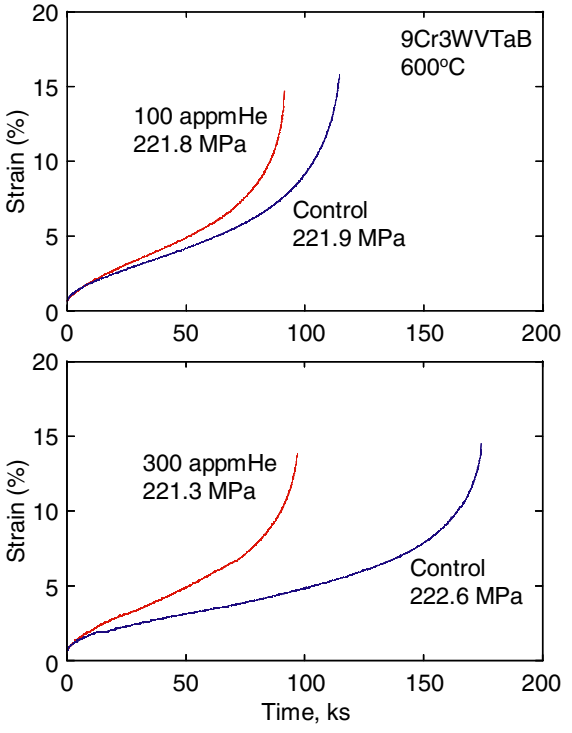

Fig. 3. Comparison of creep curves of helium-implanted specimens and corresponding controls of 9Cr3WVTaB martensitic steel tested at 600 °C.

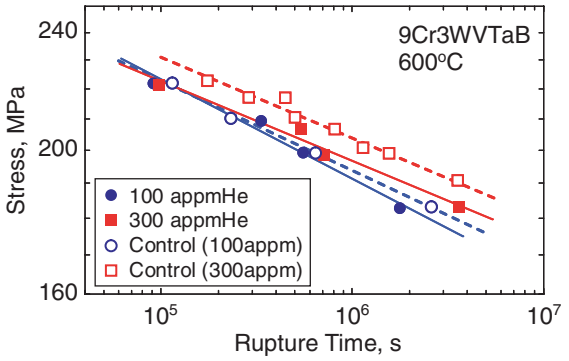

Fig. 4. Creep rupture strength as a function of creep rupture time at 600 °C for helium-implanted specimens and corresponding controls of 9Cr3WVTaB martensitic steel.

slightly reduced. It was reported for similar martensitic 9Cr–1WVTaB steel that the recovery of microstructures such as the coarsening of martensite lath subgrains during creep rupture testing at 600 °C for about 7.2 Ms was strongly suppressed by the small addition of V, Ta and B [9]. Shiba et al. investigated the thermal aging effects on tensile properties of 8Cr–2W–VTa steel (F82H) [10]. Their results exhibited no changes both in strength and elongation after 600 °C aging for 3000 h. Therefore, it is unlikely that difference in thermal histories in this investigation affects the creep rupture properties, although aging time of control samples corresponding to 300 appmHe implantation was about three times longer than that of 100 appmHe implantation. On the other hand, the usual variation of creep rupture times in thin specimens is at least a factor of 2 [11]. Differences in creep lifetimes among all samples normally accorded within the usual variation. Therefore, influence of helium on the creep lifetime is considered insignificant up to 300 appmHe. All the data in Fig. 4 were fitted to a creep power law of creep lifetime, $t_r \propto \sigma^{-n}$, and obtained stress exponents (n) are summarized in Table 1. There was noticed no significant difference in the stress exponents for all test series. This result reveals that creep mechanism would not be changed by helium implantation.

Dependence of the minimum creep rate on applied stress is presented in Fig. 5. Though the minimum creep rate of control samples corresponding to 300 appmHe

Table 1
Stress exponent (n) of creep power law fitting for creep lifetime, $t_r \propto \sigma^{-n}$, for helium-implanted specimens and corresponding controls of 9Cr3WVTaB martensitic steel creep tested at 600 °C

	Implanted	Control
100 appmHe	14.9	16.5
300 appmHe	18.6	18.4

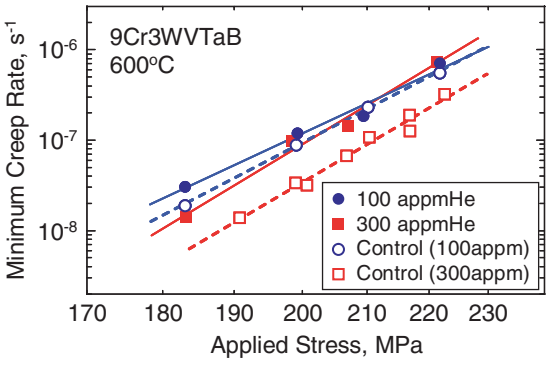

Fig. 5. Minimum creep rate as a function of applied stress at 600 °C for helium-implanted specimens and corresponding controls of 9Cr3WVTaB martensitic steel.

implantation was, mirroring the creep lifetime shown in Fig. 4, somewhat smaller than the others, difference between implanted and unimplanted specimens does not seem to be significant. The results of the statistical analysis on the creep power law for the minimum creep rate, $\dot{\varepsilon}_{MCR} \propto \sigma^m$, are listed in Table 2. The stress exponents (m) of implanted and unimplanted cases were comparable for each helium concentration. This result also reflects that helium implantation virtually caused no detrimental effect on the minimum creep rate.

The creep rupture elongation is plotted in Fig. 6 as a function of creep rupture time for all specimens tested. There were little differences in the rupture elongation on the average, and mean values were ranging from 12% to 14%. It is obvious that rupture elongation was hardly affected by helium. Because of large scatter of data, it is difficult to identify any dependence of rupture elongation on rupture time.

Fig. 7 shows typical fracture surfaces of implanted specimens and corresponding controls for both helium

Table 2
Stress exponent (m) of creep power law fitting for minimum creep rate, $\dot{\varepsilon}_{MCR} \propto \sigma^m$ for helium-implanted specimens and corresponding controls of 9Cr3WVTaB martensitic steel creep tested at 600 °C

	Implanted	Control
100 appmHe	15.9	17.6
300 appmHe	20.4	19.8

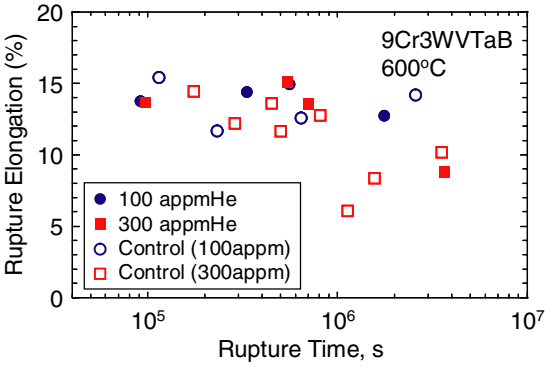

Fig. 6. Creep rupture elongation as a function of creep rupture time at 600 °C for helium-implanted specimens and corresponding controls of 9Cr3WVTaB martensitic steel.

contents, which crept at the equivalent level of applied stress. All the samples failed in a perfectly transgranular ductile manner showing a mixture of the wedge type fracture (Fig. 6(a), (c), (e) and (g)) and the dimple pattern (Fig. 6(b), (d), (f) and (h)). There was no indication of intergranular decohesion induced by helium. It was pointed out in previous literature [12,13] that detrimental helium effects resulted in not only enhancing intergranular fracture but also suppressing necking in

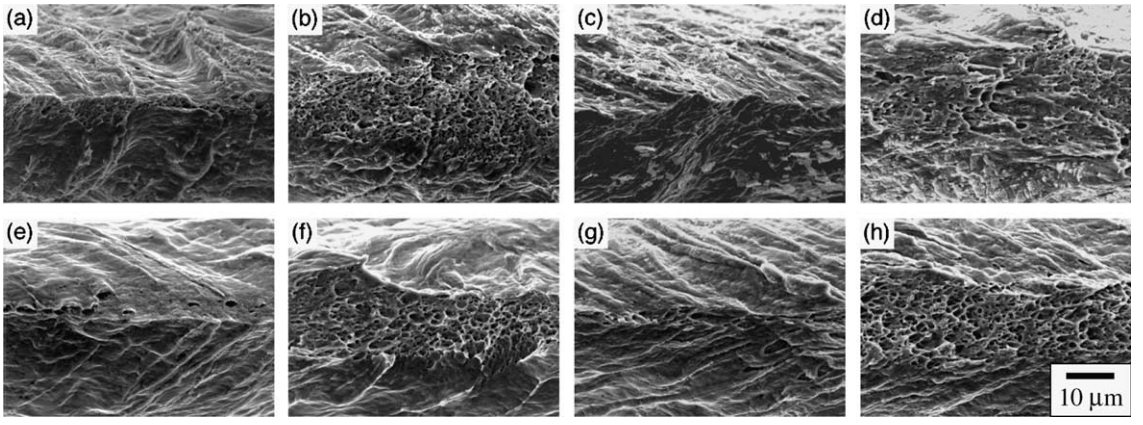

Fig. 7. Typical fracture surfaces of 9Cr3WVTaB martensitic steel creep-tested at 600 °C, 199 MPa; helium-implanted specimens up to (a), (b) 100 appmHe, (c), (d) 300 appmHe, control specimens corresponding to (e), (f) 100 appmHe implantation, (g), (h) 300 appmHe implantation.

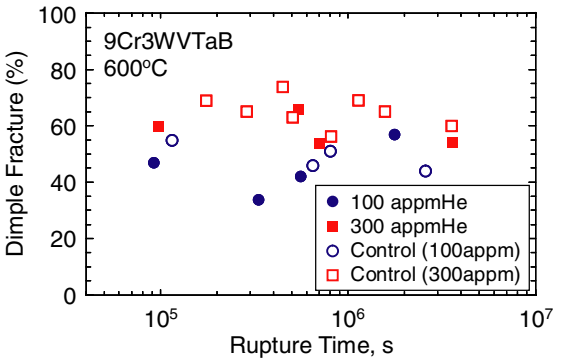

Fig. 8. Fraction of dimple fracture regions on creep rupture surfaces as a function of creep rupture time at 600 °C for helium-implanted specimens and corresponding controls of 9Cr3WVTaB martensitic steel.

ductile fracture. In order to examine the influence of helium on ductile fracture, the fraction of dimple fracture regions were evaluated on the basis of line analysis using a series of SEM fractographs. The results are plotted in Fig. 8 as a function of creep rupture time. Though scatter of the results was large, increase in dimple fracture regions by helium was not recognized.

4. Summary

Helium effects on creep rupture behavior of 9Cr3WVTaB martensitic steel were examined by means of homogeneous helium implantation at an accelerator and a series of post implantation creep rupture tests at 600 °C.

(1) There was little difference in creep rupture time between implanted and unimplanted specimens when helium was introduced at 100 appm. Though creep rupture time of implanted samples slightly reduced in comparison with corresponding controls in case of 300 appmHe implantation, the reduction was within the usual variation of creep rupture time of a factor of 2.
(2) Creep rupture elongation was hardly affected by helium and mean values of the creep rupture elongation were between 12% and 14% regardless of whether helium was introduced or not.
(3) All the specimens containing up to 300 appmHe failed in a perfectly intragranular ductile manner without any indication of grain boundary separation induced by helium. The fraction of dimple fracture regions in ductile fracture faces was hence hardly changed by helium implantation.

Acknowledgements

This study was financially supported by the Budget for Nuclear Research of the Ministry of Education, Culture, Sports, Science and Technology, based on the screening and counseling by the Atomic Energy Commission.

References

[1] B. van der Schaaf, D.S. Gelles, S. Jitsukawa, A. Kimura, R.L. Klueh, A. Möslang, G.R. Odette, J. Nucl. Mater. 283–287 (2000) 52.
[2] E. van Osch, M.G. Horsten, G.E. Lucas, G.R. Odette, in: M. L. Hamilton, A.S. Kumar, S.T. Rosinski, M.L. Grossbeck (Eds.), Proceedings of 19th International Symposium on Effects of Radiation Materials, ASTM STP 1366, West Conshohocken, PA, 2000, p. 612.
[3] A. Kohyama, A. Hishinuma, D.S. Gelles, R.L. Klueh, W. Dietz, K. Ehrlich, J. Nucl. Mater. 233–237 (1996) 138.
[4] R. Schaublin, M. Victoria, J. Nucl. Mater. 283–287 (2000) 339.
[5] K. Matsumoto, T. Kataoka, J. Nucl. Mater. 67 (1977) 97.
[6] N. Yamamoto, J. Nagakawa, H. Shiraishi, H. Kamitsubo, I. Kohno, T. Shikata, J. Nucl. Sci. Technol. 28 (1991) 1001.
[7] N. Yamamoto, Y. Murase, J. Nagakawa, K. Shiba, J. Nucl. Mater. 307–311 (2002) 217.
[8] N. Yamamoto, J. Nagakawa, K. Shiba, Key Eng. Mater. 171–174 (2000) 115.
[9] F. Abe, T. Noda, M. Okada, J. Nucl. Mater. 195 (1992) 51.
[10] K. Shiba, M. Suzuki, A. Hishinuma, J. Nucl. Mater. 233–237 (1996) 309.
[11] H. Schroeder, J. Nucl. Mater. 141–143 (1986) 476.
[12] U. Stamm, H. Schroeder, J. Nucl. Mater. 155–157 (1988) 1059.
[13] A. Hasegawa, N. Yamamoto, H. Shiraishi, J. Nucl. Mater. 202 (1993) 266.